Published in final edited form as:
J Control Release. 2013 November 28; 172(1): . doi:10.1016/j.jconrel.2013.06.039.

Biodistribution and Bioimaging Studies of Hybrid Paclitaxel Nanocrystals: Lessons Learned of the EPR Effect and Image-Guided Drug Delivery

Christin P. Hollis[a], **Heidi L. Weiss**[b], **Markos Leggas**[a], **B. Mark Evers**[c], **Richard A. Gemeinhart**[d], and **Tonglei Li**[e,*]

[a] Department of Pharmaceutical Sciences, College of Pharmacy, University of Kentucky, Lexington, KY 40536, USA

[b] Biostatistics, Division of Cancer Biostatistics, Markey Cancer Center, University of Kentucky, Lexington, KY 40506, USA

[c] Department of Surgery and Markey Cancer Center, University of Kentucky, Lexington, KY 40506, USA

[d] Departments of Biopharmaceutical Sciences, Bioengineering, and Ophthalmology and Visual Sciences, University of Illinois, Chicago, IL 60612

[e] Department of Industrial and Physical Pharmacy, College of Pharmacy, Purdue University West Lafayette, IN 47907, USA

Abstract

Paclitaxel (PTX) nanocrystals (200 nm) were produced by crystallization from solution. Antitumor efficacy and toxicity were examined through a survival study in a human HT-29 colon cancer xenograft murine model. The antitumor activity of the nanocrystal treatments was comparable with that by the conventional solubilization formulation (Taxol®), but yielded less toxicity as indicated by the result of survival study. Tritium-labeled PTX nanocrystals were further produced with a near infrared (NIR) fluorescent dye physically integrated in the crystal lattice. Biodistribution and tumor accumulation of the tritium-labeled PTX nanocrystals were determined immediately after intravenous administration and up to 48 hours by scintillation counting. Whole-body optical imaging of animals was concurrently carried out; fluorescent intensities were also measured from excised tumors and major organs of euthanized animals. It was found that drug accumulation in the tumor was less than 1% of 20 mg/kg intravenous dose. Qualitatively correlation was identified between the biodistribution determined by using tritium-labeled particles and that using optical imaging, but quantitative divergence existed. The divergent results suggest possible ways to improve the design of hybrid nanocrystals for cancer therapy and diagnosis. The study also raises questions of the general role of the enhanced permeability and retention (EPR) effect in tumor targeting and the effectiveness of bioimaging, specifically for hybrid nanocrystals, in tracking drug distribution and pharmacokinetics.

*Correspondence to: Tonglei Li Department of Industrial and Physical Pharmacy College of Pharmacy, Purdue University Heine Pharmacy Building 575 Stadium Mall Drive West Lafayette, IN 47907, USA Tel: 765-494-145 Fax: 765-494-654 tonglei@purdue.edu.

Keywords

paclitaxel; nanocrystals; hybrid; theranostics; chemotherapy; EPR; biodistribution

1. Introduction

Many anticancer compounds are poorly soluble in aqueous solutions. To enhance solubility, these compounds are further compounded by chemicals and solvents. Furthermore, these cytotoxic compounds can damage normal tissues and organs when given to patients systematically. Over the last decade, significant efforts have been undertaken to develop nanosized drug delivery vehicles as a tumor-targeting strategy, in which anticancer compounds can be solubilized and encapsulated. The impetus to develop nanoparticle based cancer therapy has been the enhanced permeation and retention (EPR) effect [1,2] that facilitates the passive accumulation of particles (20-200 nm) in tumor tissues. This effect is due to the rapid and disorganized growth of tumor blood vessels, which have abnormally large interendothelial pores that allow for particle extravasation [3,4]. On the other hand, diffusion of solubilized drugs into the tumor is impeded by the poor convective flow of interstitial fluids due to lacking of lymphatic system as tumor grows. Thus, it is postulated nanoparticles may provide a better delivery approach as they extravasate from the leaky vasculature and localize in the tumor allowing for increased drug concentrations at the action site. As the extravasation process relies on adequate numbers of nanoparticles being present in the circulation, nanoparticles are often pegylated to attenuate their clearance by the macrophage phagocytic system, which allows for their prolonged circulation.

Despite the popularity of the EPR effect in promoting nanomedicine research, questions have been raised regarding how significant or reliable the effect is. Based on assessment of literature data on the tumor accumulation of nanoparticles for cancer therapy, it is argued that no more than 5% of the injected dose extravasates and accumulates in tumors [5]. The extent of nanoparticle extravasation depends heavily on the interendothelial pore size, which varies among tumor types and histological grades [6-8]. For example, certain tumors, such as metastatic liver and prostate cancer, bear intrinsically low vascular densities [9], in which the EPR effect strategy may not apply in the core of a large-sized tumor (e.g., 1-2 cm in diameter) due to the absence of densely vascularized structures [10]. The hypoxic nature of the tumor generally leads to the formation of necrotic tissues further preventing the access by nanoparticles. Therefore, it becomes imperative to have a clear understanding of the tumor accumulation, as well as the biodistribution and pharmacokinetics, when developing a nanoparticle-based delivery system. Such knowledge is invaluable in further optimizing and evaluating the delivery system with respect to the treatment efficacy and systematic toxicity.

Among various nanomedicine designs, nanocrystal formulation has been explored for delivering antineoplastic agents. Nanocrystals can be produced either by top-down or bottom-up approaches [11-13]. Besides existing as the most stable, crystalline state, nanocrystals typically carry nearly 100% drug loading and can be directly administered as solid particles intravenously. Compared with conventional solubilized delivery systems, nanocrystals induce much less systemic toxicity and can thus be given at a higher dose in order to achieve better therapeutic efficacy [14,15]. What has been pursued in our laboratory is a nanocrystal design in which imaging agents are physically integrated or entrapped in the crystal lattice of drug nanocrystal hosts [16]. These hybrid nanocrystals aim to simultaneously achieve anticancer treatment and bioimaging, offering a simple and potentially versatile platform of theranostics.

Incorporation of bioimaging agents into traditional encapsulation delivery systems has been investigated, including liposomes [17], polymersomes [18], polymeric nanoparticles [19], and micelles [20]. The integrated imaging probes permit non-invasive tracking *in vivo* and in real-time, potentially enabling longitude evaluation of tissue distribution, pharmacokinetics, and therapeutic response. Amongst the available bioimaging modalities [21,22], optical imaging have been mostly investigated in the pre-clinical studies due to its ease of operation, high sensitivity, low running cost, and absence of radioactive irradiation [23,24]. This modality has also been explored as a screening tool to evaluate the tumor targeting efficiency of formulations having different physicochemical properties [25-30]. Nonetheless, limitations still exist in these designs, including low drug loading efficiency and capacity [31], vehicle instability and drug leakage [32,33].

Despite the significant therapeutic improvement by nanocrystals, assessment of the *in vivo* performance of nanocrystal injection remains largely limited. In particular, the knowledge of biodistribution and tumor accumulation of nanocrystals is scarce. More importantly, it almost remains unknown how hybrid nanocrystals function *in vivo* as a potential theranostic platform. As such, tritium-labeled PTX nanocrystals in which an optical dye was physically integrated were evaluated in a mouse xenograft model. In particular, tissue distribution and tumor accumulation of the PTX hybrid nanocrystals were analyzed and correlated by both scintillation and bioimaging. The objectives of the study included (a) to investigate the efficacy and toxicity of Taxol and PTX nanocrystals by examining the survival of mice treated by respective delivery systems, (b) to measure and compare the biodistribution and tumor accumulation of ^{3}H-Taxol and ^{3}H-PTX hybrid nanocrystals in mice, and (c) to image the mice treated by the hybrid nanocrystals and assess the bioimaging results based on the biodistribution results by the isotope analysis. The measurements were performed in athymic mice with HT-29 colon cancer xenograft implanted in the flank sites.

2. Materials and Methods

2.1. Materials

Paclitaxel (>99.5%, USP30) was purchased from 21CECPharm (United Kingdom). Tritium-labeled paclitaxel (^{3}H-PTX) in ethanol (≥ 97% chemical purity, 4 mCi/mmol, 0.145 mCi/mL) was purchased from Moravek Biochemicals and Radiochemicals (Brea, CA). FPI-749 fluorophore (maximum excitation wavelength, λ_{ex}=750 nm; maximum emission, λ_{em}=782 nm) was obtained from Akina LLC (West Lafayette, IN). Ethanol (HPLC grade), acetonitrile (HPLC grade), fetal bovine serum, penicillin streptomycin, and 0.25% trypsin-ethylenediaminetatraacetic-acid (EDTA) were purchased from Fisher Scientific (Pittsburgh, PA). Saline (0.9% w/v sodium chloride) for injection was obtained from Hospira (Lake Forrest, IL). All chemicals and solvents were utilized without further purification. HT-29 human colon adenocarcinoma cells and McCoy's 5A medium were purchased from ATCC (Manassas, VA). Deionized water (by Milli-Q®, filtered through 0.2 μm membrane) was used for all the experiments. 50 nm-Whatman® Nuclepore polycarbonate track-etched membranes used for filtration were purchased from Fisher Scientific (Pittsburgh, PA).

2.2. Preparation of Pure PTX Nanocrystals and Taxol Formulation

Paclitaxel pure nanocrystals were produced by crystallization. Subsequent to precipitation via an anti-solvent approach [16], the suspension was subjected to homogenization for 6 minutes in order to enhance the particle size uniformity. PTX nanocrystals were purified and concentrated through a few filtration-rinsing-resuspension cycles; the resultant suspension was stored in DI water at 4°C. Prior to each intravenous injection, the PTX nanosuspension was diluted with saline to achieve a concentration of 3 mg/mL. The Taxol formulation was

prepared by dissolving PTX into a 50:50 mixture of ethanol and Cremophor EL®; for injection, the stock solution was diluted with saline to obtain a concentration of 3 mg/mL.

2.3. Characterization and Analysis of PTX Nanocrystals

Scanning electron micrographs were obtained by a Hitachi SEM 4300 (Hitachi High Technologies America, Inc., Schaumburg, IL) at accelerating voltage of 3 kV. The samples were sputter-coated with conductive layers of gold palladium (Au/Pd) for 1 minute at the current of 20 mA. The longest dimension of the particles was estimated by SigmaScan (Systat software, San Jose, CA), and the mean ± S.D. (standard deviation) was calculated. The hydrodynamic diameter and zeta potential were measured in deionized water and 10 mM NaCl, respectively, using a dynamic light scattering (DLS) system, Malvern Nano-ZS Zetasizer (Worcestershire, United Kingdom). Chemical quantification of PTX was conducted by a high-pressure liquid chromatography (HPLC, Waters Breeze, Milford, MA) with a C18 5 μm column (4.6 × 150 mm) and a UV detector at 227 nm. Acetonitrile and water (50:50) were pumped at a total flow rate of 2 mL/min. The column was equilibrated to 35 °C prior to sample injection (20 μL) prior to sample injection (20 μL) of nanocrystal suspension diluted in ethanol at a volume ratio of 1:100.

2.4. Preparation and Analysis of ^{3}H-Taxol and ^{3}H-PTX/FPI-749 nanocrystals

Tritium-labeled Taxol formulation (^{3}H-Taxol) was prepared by spiking the solution containing PTX at 30 mg/mL in a 50:50 (v/v) mixture of Cremophor EL and ethanol with ^{3}H-PTX and reaching the radioactivity of 2.058 mCi/mmol. Prior to the intravenous injection, the stock was diluted with saline to reach a final concentration of 3 mg/mL.

^{3}H-PTX/FPI-749 hybrid nanocrystals were produced by the same approach used in the production of pure nanocrystals mentioned above. Specifically, 0.7 mL of 1 mg/mL FPI-749 was added to 20 mL deionized water in a 3-neck flask. 1 mL of 5 mg/mL (2.058 mCi/mol) of ^{3}H-PTX in ethanol was then added rapidly to the flask. The mixture was stirred with a stirrer shaft and under intense sonication (F20D, Fisher Scientific, Pittsburgh, PA). The flask was removed from the stirring station and subjected to vacuum to remove excess bubbles generated by stirring. The mixture was then filtered through a 50-nm polycarbonate membrane. The retentate was rinsed and re-suspended in water for additional filtration-re-suspension cycles to remove any loosely bound fluorophores. The suspension was further homogenized (Fisher Scientific PowerGen® 125, Pittsburgh, PA) to enhance the particle size uniformity. A separate batch of PTX hybrid nanocrystals without ^{3}H-PTX was produced for scanning electron microscopy. To quantitate the radioactivity in the injection, three 10 μL aliquots from the suspension were analyzed by a liquid scintillation counter, Tri-Carb 2910TR (Perkin Elmer, Waltham, MA).

2.5. HT-29 Cell Culture

HT-29 human colon adenocarcinoma cells were cultured in McCoy's 5A medium supplemented with 10% fetal bovine serum and 1% penicillin streptomycin in a humidified incubator containing 5% CO_2 at 37 °C. To establish the HT-29 xenograft in nude mice, HT-29 cells were harvested (by using 0.25% trypsin-EDTA) when the cells became 70-90% confluent. The cells were suspended in a 50:50 mixture of sterile phosphate buffered saline (PBS) and Matrigel (BD Biosciences, San Jose, CA) at a concentration of 3×10^{7} cells/mL. Cell suspensions were kept in ice before the inoculation.

2.6. Antitumor Activity and Treatment Toxicity

The animal study was conducted under a protocol approved by the University's Institutional Animal Care and Use Committee (IACUC). Female nude outbred mice (Tac:Cr: (NCr)-

Foxn1 Nu) were obtained from Taconic at 4 weeks of age (14.5-20 g). Mice were acclimated for one week after arrival. Subsequently, under anesthesia, each animal was identified by pinching a tag to the ear and inoculated with 100 μL HT-29 cells (3×10^6) injected subcutaneously to both sides of flank, respectively. The mice were monitored three times every week with respect to body weight, tumor volume, and overall morbidity. The tumor volume from each side of the flanks was measured by a digital caliper and calculated as longest dimension × (shortest dimension)^2 / 2 and summed for the total tumor volume per animal. Tumors became palpable (100-300 mm^3) after nine days of inoculation. A total of 36 mice were randomized into 3 groups to be treated respectively by saline (control), Taxol, and pure PTX nanocrystals. Intravenous injections of Taxol and PTX nanocrystals were administered at the dose of 20 mg/kg via tail vein weekly on days 10, 17, 24, and 31 after the cell inoculation; correspondingly, 150 μL of saline was administered to the control group. Through the survival study, the endpoint was determined when an animal met one of the following conditions: (i) it became moribund, (ii) the tumor reached 1,500 mm^3 in size, became ulcerated, or impeded its ability to attain food or water, (iii) it lost 20% of their body weight, and (iv) it developed severe medical condition or adverse effects.

2.7. Tumor Accumulation and Biodistribution

The animal study was conducted under the same protocol as described above. A total of 111 athymic mice were randomized and grouped. Three mice were allocated to receive no treatment (control). For the ^{3}H-Taxol-treated group, 48 mice were allocated into 12 time points (n = 4) accordingly: 5, 15, 30 minutes, 1, 2, 4, 6, 8, 24 hours, 2, 3, and 4 days. For the ^{3}H-PTX hybrid nanocrystals-treated group, 60 mice were divided into 15 time points (n = 4): 11, 15, 30 minutes, 1, 2, 4, 6, 8, 24 hours, 2, 3, 4, 5, 6, and 7 days. ^{3}H-Taxol and ^{3}H-PTX/FPI-749 nanocrystals were diluted in saline and respectively administered intravenously once at an equivalent dose of 20 mg/kg via the tail vein. Each mouse received approximately 1 μCi of tritium via the injection.

The animals in the PTX hybrid nanocrystal group were imaged by IVIS® Spectrum (Perkin Elmer, Waltham, MA). Due to transportation and imaging duration, the first time point at which animals could be euthanized was 11 minutes. Mice were euthanized at pre-determined time points by CO_2 asphyxiation. After performing cervical dislocation, blood, tumor from both sides of the flank, and major organs were collected, washed with DI water, and weighed in pre-weighed scintillation vials before further analyses.

2.8. Tritium Analysis of Blood and Tissues

Blood and tissue samples were prepared according to the scintillation analysis protocol provided by Perkin Elmer. Specifically, a blood sample (0.1-0.4 mL) was treated by 1 mL of a mixture (1:1 v/v ratio) of tissue solubilizer Soluene® 350 (Perkin Elmer, Waltham, MA) and ethanol prior to being incubated in a 50-60°C oven for at least 2 hours. Cooled back to room temperature, the sample was decolorized by 500 μL of 30% hydrogen peroxide solution. Once the decoloration reaction subsided, the sample was placed back in the oven for another 30 minutes. 15 mL of liquid scintillation cocktail (Perkin Elmer) was added to the blood sample and the mixture was vortexed before being quenched for 1 hour in the dark. The sample was then measured by a liquid scintillation counter.

Tumor and tissue samples were homogenized before the scintillation measurement. 50-200 mg of a homogenized tumor or tissue sample were digested with Soluene 350 and incubated in an oven at 50-60°C for about 4 hours. Cooled back to room temperature, a sample was decolorized with 200 μl of 30% hydrogen peroxide. Once the reaction was completed, the sample was placed back in the oven for another 30 minutes. 15 mL and 10 mL of Hionic-

Fluor were added to the blood and tissue samples, respectively, prior to quenching in the dark for 1 hour. The sample was measured by a liquid scintillation counter.

2.9. Bioimaging

The mice treated by the PTX/FPI-749 hybrid nanocrystals were imaged by IVIS Spectrum at predetermined time points. The animals were imaged either from the dorsal or ventral side under anesthesia. The following parameters were used for the imaging: $\lambda_{excitation}$ = 745 nm, $\lambda_{emission}$ = 800 nm, exposure time = 4 seconds, F stop = 2, binning = medium (8), and field of view (FOV) = 13. Tumor and major organs from euthanized animals were also imaged under the same set of parameters.

2.10. Statistical Analysis

Kaplan-Meier curves were generated for each treatment group and the comparison of overall survival across treatment groups was performed by the log-rank test. Median time and the percentage of survival at specific time point were estimated from the Kaplan-Meier curves. Body weight change was plotted for each group. Pairwise comparison at each time point of follow-up was calculated by the non-parametric Wilcoxon rank-sum test to account for non-normality of the data. The tumor accumulation at specific time points between groups was evaluated by analysis of variance, which included treatment group, time point, and interaction between these two factors in the model.

3. Results and Discussion

3.1. Characterization of Pure and Hybrid PTX nanocrystals

Representative nanocrystal samples are shown in Figure 1. The averaged longest dimension of the crystals was 200 nm estimated based on SEM images. The nanocrystals resembled a well-defined, short, rod-like morphology. Summarized in Table 1 are the physical properties of pure PTX nanocrystals used in the survival study. Because of a low aspect ratio and narrow particle size distribution, as suggested by the polydispersity indices, particle size values measured by DLS agreed fairly well with those estimated from SEM. The particle size of PTX nanocrystals utilized for injection 1, however, was significantly smaller ($p<0.05$) than those used for other injections (i.e., 2, 3, and 4). The zeta potential of PTX nanocrystals (0.1 mg/mL) was measured as -9.8 ± 0.5 mV in 10 mM NaCl at 25 °C. To minimize possible agglomeration and reduce Ostwald Ripening, nanocrystals should be stored at 4 °C or freeze-dried.

Particle size is known to have impact on clearance and tumor uptake [5]. It is shown that smaller particles (e.g., 50-300 nm) are commonly removed from the circulation relatively slowly [34,35]. It is however difficult to generalize an optimal particle size to maximize the exploit of the EPR effect, due to tumor heterogeneity as well as variations in particle properties (e.g., size, shape, and surface charge) [7,8]. Nonetheless, it seems to be well accepted that nanoparticles with the size up to 400 nm are able to take advantage of the EPR effect [5,36]. To that end, by varying and optimizing growth conditions, nanocrystals of 200 nm were produced and utilized in this study.

3.2. Antitumor Efficacy and Treatment Toxicity

Nine days after the subcutaneous implantation of HT-29 cells to a total of 36 mice, tumor xenografts became palpable. The animals were randomized equally into three groups and treated by four weekly injections of saline, Taxol, and PTX nanocrystals, respectively. The endpoint of the study was met on day 32 when all of the mice in the control group had to be euthanized due to tumor size. The Kaplan-Meier survival curves were plotted in Figure 2A. For those animals in the treatment groups that were euthanized before the end of the study,

their tumors either exceeded 1500 mm^3 or their weight loss was significant (more than 20%). The survival probability on day 30 of the control, Taxol, and PTX nanocrystal groups were 16.7%, 66.7%, and 83.3%, respectively. The mice in the control group reached the median survival time by day 25, while the median survival time was not reached for the Taxol and PTX nanocrystal group when the study ended.

Furthermore, the log-rank analysis revealed that there was significant difference in treatment efficacy between the control and Taxol groups ($p = 0.003$) as well as the control and PTX nanocrystal groups ($p = 0.001$). There was no significant difference, however, between the two treatment groups ($p = 0.970$). In addition, body weight was monitored through the survival study (Figure 2B). Upon statistical analysis, the differences in the body weight change between the two treatment groups were significant ($p < 0.05$) on days 16 and 23 (i.e., the 6^{th} day after weekly injections) when the number of animals in each group was identical ($n = 12$). It is worth noting that, on the final day, day 32, 4 out of 8 mice in the Taxol group had body weight loss of more than 5%, compared to just 1 out of 8 mice in the PTX nanocrystal group. While the control and Taxol groups had similar weight loss profiles (Figure 2B), the former had much poorer survival (Figure 2A). On the other hand, both Taxol and nanocrystal groups showed similar survival traits and, yet, the former had significant weight loss. Thus, the results suggest that the body weight loss likely resulted from the solvent-induced toxicity. In spite of the similar efficacy when administered at 20 mg/kg, PTX nanocrystals offered safer delivery of PTX; higher dose may be warranted [37].

3.3. Tissue Distribution by Tritium Analysis

Tissue distribution of the drug in mice was analyzed through tritium-labeling and scintillation counting. The conventional formulation, Taxol, has previously been shown to distribute extensively to all major organs and to exhibit a non-linear, two compartmental, pharmacokinetic profile [38,39]. The extensive tissue distribution of the drug and solubilizing agents can potentially induce profound toxic effects, as suggested by the body weight change (Figure 2B). Compared with the solubilized formulation, ^{3}H-PTX nanocrystals were cleared rapidly from the blood circulation. By 15 minutes after injection, only $0.42 \pm 0.12\%$ of PTX per gram of blood was detected as opposed to $2.89 \pm 0.24\%$ of ^{3}H-Taxol. This is in accordance with previous studies that have suggested that the surfactant used in Taxol, Cremophor EL, could form micelles and solubilize the drug [40] and may also allow free drug molecules to partition reversibly in circulating surfactants [41].

With respect to ^{3}H-PTX nanocrystals, the significant decrease in blood concentrations contrasted with high drug concentrations in liver, spleen, and lungs suggest that nanocrystals were sequestered by the macrophages of the macrophage phagocytic system (MPS) within minutes of intravenous administration. Despite the fact that close to 40% of the injected dose was taken up by the liver, it seems that the entrapment of the nanocrystals in liver, most likely by Kupffer cells, does not necessarily lead to significant adverse effects, especially compared with the conventional solubilized formulation. An earlier study showed that itraconazole nanocrystals after intravenous administration were engulfed by macrophages and resided within the cytoplasm; the number of resident macrophages was also increased to accommodate the particle burden when the dose was elevated [42]. Clearly, if the MPS uptake of the nanocrystals does not result in significant toxicity, higher dose may be possible, and liver may temporarily act as a depot site to release the drug back into the circulation. Compared with the ^{3}H-Taxol distribution (Figure 3A), ^{3}H-PTX/FPI-749 nanocrystals were distributed rapidly to the major organs within the first 11 minutes (Figure 3B). Nonetheless, Figure 3B suggested the free ^{3}H-PTX was redistributed from the clearing organ (i.e., liver) back to the systemic circulation, especially at the 1- and 6-hour time points. The decreased mean concentration of ^{3}H-PTX in the liver was accompanied with an increased mean concentration in the blood. This observation suggests that there was higher

concentration of ^{3}H-PTX that was redistributed than being cleared. Conversely, subsequent to the intravenous injection of ^{3}H-Taxol, ^{3}H-PTX concentration in the blood circulation continually decreased.

The relative amounts of the drug out of every injection in the major organs and tumor were also analyzed for both ^{3}H-Taxol and ^{3}H-PTX nanocrystals (Figures 4A and 4B). Within the first 10-15 minutes, the total percentage of PTX in the major organs and tumor was only summed up to approximately 50%. The remainder of the injected dose was largely distributed in other tissues, likely due to the lipophilic nature of the drug. It is striking to see that less than 1% of the drug accumulated in the tumor. The comparison of tumor accumulation between the two formulations will be further discussed later.

The nanocrystals used in the study were bare, without any functionalization or adsorption by surfactants or polymers. Pegylation is a common practice to circumvent or delay the recognition by the MPS, possibly due to the hydrophilic polymer shell that prevents opsonins from attaching to the surface and subsequent phagocytosis [43,44]. There are a few studies where drug nanocrystals were stabilized by PEG or PEG block polymers but they were still sequestrated in MPS significantly [45-47]. Clearly, it is a challenging task to secure surfactants to the surface of nanocrystals, especially during the administration and blood circulation stages.

3.4. Tumor Accumulation

Tumor accumulations of the solubilized and nanocrystal formulations are plotted together for comparison (Figure 4 inset). The values reached the maximum during 1 to 6 hours after injection. Statistically, the tumor accumulation of ^{3}H-Taxol was significantly higher than that of ^{3}H-PTX nanocrystals regardless of the time point ($p < 0.0001$). Furthermore, the statistical interaction between the group and time variables was not significant ($p = 0.182$), indicating that there was a consistent difference between the treatments across all time points.

A major reason for the low tumor accumulation by the nanocrystals obviously lies in the short duration in the blood circulation and the quick sequestration by MPS. Elevated tumor intersitial pressure and unique vasculatures of HT-29 xenograft may also be responsible. HT-29 tumors were reported be less vascular, for example, than the human colon adenocarcinoma LS174T [48]. Conversely, the relatively high intratumoral accumulation of ^{3}H-Taxol may be ascribed to the micellar encapusulation by Cremophor EL [40]. Nonetheless, the tumor accumulation of ^{3}H-Taxol continued to decrease after 6 hours, corresponding well with the blood concentration profile. The clearance of the drug from the tumor was likely facilitated by partitioning PTX reversibly into the circulating Cremophor EL [41]. Interestingly, the tumor accumulation of ^{3}H-PTX nanocrystals after 6 hours was steadily maintained. It is likely that, once the nanocrystals successfully accumulated in the tumor site, they would not be cleared easily due to relatively large particle size and ineffective lympathic drainage surrounding the tumor. Also as pointed out earlier, it is possible that the sequestered nanocrystals in MPS continued to dissolve releasing PTX molecules (and even smaller particles) back to the blood stream and maintaining the drug concentration in the tumor. The finding of initial sequestration of nanoparticules by phagocytosis followed by slow release is commonly observed [35]. Relative to solution formulation, nanocrystals are shown to have prolonged half-lives of elimination in murine models [45-47,49,50]. Thus, it is highly possible that, upon multiple injections, drug accumulation in the tumor will become significant, as demonstrated by the treatment regimen in the survial study discussed above.Needless to say, the EPR effect as observed in this study was minimal. If the Taxol formulation may be regarded as a nanoparticle delivery system because of the possible micellar encapsulation of PTX, both nanosystems were

"leaked" out to the tumor less than 1% of the total injected dose. In addition, the particle size of the nanocrystals (*ca*. 200 nm) may be at the upper limit to take advantage of possible EPR effect. Limited blood circulation time and engulfment of nanocrystals by macrophages may also contribute to the minimal EPR effect observed.

3.5. Whole-Body Fluorescence Imaging

The feasibility and performance of ^{3}H-PTX/FPI-749 nanocrystals as an optical imaging system were evaluated *in vivo*. Mice injected with the hybrid nanocrystals were imaged at the predetermined time points with an IVIS system from both the dorsal and ventral sides (Figures 5 A and B). Three mice were allocated as control (no treatment). Apparently, strong peripheral fluorescence signals were detected within the first few hours after injection. There was also an increase in the fluorescence ratio between the tumor and peripheral areas starting after 1 hour (Figure 5A). This seems to be supported by the tumor accumulation data of the tritium-labeled drug that maximized at 1 hour (Figure 4 inset). The tumor was significantly outstanding after 1 day and the overall intensity decreased after 5 days. From the ventral side, the strongest intensity came from the liver area within a few minutes of intravenous injection and remained the most outstanding throughout the observation period (Figure 5B). After 30 minutes, intensity in the bladder area increased steadily for about 4 hours, indicating urinary clearance of the dye. The flank areas were also noticeable particularly after 8 hours. The overall intensity became trivial after 5 days.

Nonetheless, discrepancies existed between the biodistribution results determined by tritium labeling and what the whole-body fluorescence imaging indicated. This is particular true for the tumor. The imaging data pointed out the tumor being a strongly fluorescent area. The discrepancies could be caused by several reasons. First, the fluorescent signal is a summation of the contributions by both entrapped and freely dissolved dyes. When a hybrid nanocrystal dissolves, it releases both free drug and dye molecules. Consequently, when most nanocrystals remained un-dissolved, a fluorescent image corresponds closely to where nanocrystals reside; when the nanocrystals start to dissolve, the difference in biodistribution between PTX as measured by scintillation counting and fluorescence images is expected to become larger. For instance, fluorescent signal observed in the liver was mainly due to the hybrid nanocrystals because it coincided with isotope accumulation in the site within a few minutes. Conversely, that of the tumor may be generated from the free dye because the tritium accumulation in the tumor was less than 1%. In addition, at 30 minutes after injection, strong fluorescent signal started to appear in the urinary bladder area, indicating that free FPI-749 molecules were renally cleared and excreted through the bladder. It was also possible that a significant number of nanocrystals started to dissolve soon after the injection. Second, because PTX is hydrophobic and the dye is hydrophilic, the two different molecules are expected to have drastically different biodistribution preferences and clearance pathways. A considerable amount of free dye molecules were accumulated in the tumor region, possibly due to concentrated blood vasculatures in the milieu. Third, the limitation in the penetration depth by fluorescence light signifies the surface layer of an animal much more than deeper tissues and organs. Light scattering and absorption by blood (oxyhemoglobin and deoxyhemoglobin) and water further attenuate the signal particularly emitted from internal organs [51].

3.6. Ex vivo Imaging

Subsequent to euthanization by CO_2 asphyxiation, the tumor and major organs were excised and imaged under IVIS (Figure 6). The total fluorescence intensities from individual organs and tumors were normalized by the weight of a tissue and shown in Figure 7. While the trends in the liver and spleen between the drug distribution and bioimaging were comparable, the fluorescent intensities in the tumor, heart, lungs, and kidneys were much

elevated. It is important to note that the fluorescence in heart, lungs, and kidneys dissipated rapidly – indicated by the steep slopes – implying that the dye molecules were cleared out of the system. In contrast, a temporal delay of clearance in tumor was observed.

The results further illustrate the limitation of using fluorescence imaging for biodistribution detections of drug delivery systems. When the dye is released from the nanocrystals, discrepancy appears. Still, coherence does exist, particularly in the liver in which 40-50% of the hybrid nanocrystals were sequestered by macrophages. Strong fluorescent signals observed also in the spleen and lungs were most likely contributed by entrapped FPI-749 from nanocrystals. As demonstrated in Figure 4B, the strong intensity in the tumor, nevertheless, likely came from released, free dye molecules – for example, from phagocytized nanocrystals – that re-entered the blood circulation. Moreover, light absorption by hemoglobin in the NIR range can present an interference factor as well [52,53]. Blood-rich organs (e.g., liver, spleen, and lungs) are known to attenuate the reflected fluorescent signal the most [51], while tumor tissues, which are less vascular or have surface-proximal vessels that are functional, do not attenuate as much.

4. Conclusion

Through the survival study, PTX nanocrystals were shown to be as effective as the conventional Taxol formulation, but offer reduced toxic effects. The ^{3}H-Taxol was extensively distributed to major organs, while ^{3}H-PTX/FPI-749 nanocrystals were rapidly cleared from the blood circulation by the MPS with more than 40% of the injected dose found in the liver. ^{3}H-Taxol was maintained in plasma longer and accumulated in the tumor at higher concentrations than ^{3}H-PTX/FPI-749 nanocrystals. Yet, the concentration of ^{3}H-PTX in tumor was maintained quite steadily from 8 to 72 hours, suggesting the prolonged retention and possible release of ^{3}H-PTX from engulfed nanocrystals in the macrophages. Still, less than 1% of the injected dose by either Taxol or PTX nanocrystals was present in the tumor at any given time points.

Discrepancies were found between the biodistribution of the drug and the fluorescent imaging of the whole body and excised tumor and tissues. Since tissues inherit different molecular compositions and structures, they are optically distinctive in light attenuation, which translated in consequential divergence in quantitative results. In addition, the observed strong fluorescent intensity in the tumor was likely contributed by dissolved free dyes that were accumulated in the region. The clearance of fluorescent molecules from the tumor was reduced, possibly resulting from the impaired lymphatic drainage.

There are a few lessons that may be learned from this study regarding further development of nanocrystal-based delivery systems, and other systems in general, for cancer therapy and diagnosis. First, the EPR effect for both the solubilized formulation and nanocrystals was similar and insignificant with regard to drug accumulation. If the tumor can be regarded as an organ of its own, the drug concentration was much less than the concentration in other major organs, especially liver, lungs, spleen, and kidneys. Obviously, the results were affected by not just the delivery system, but also by the tumor type and its biology. Still, such a low accumulation (less than 1%) could lead to tumor suppression and antitumor efficacy. Therefore, for cancer therapy, the most critical is perhaps not to get more drugs to the tumor, but to reduce drug accumulation in major organs or at least to steer the biodistribution away from key organs (e.g., heart and brain) to reduce toxic effects. It is equally important to avoid or minimize systemic side effects due to the usage of helper chemicals for solubilizing and encapsulating a drug substance, for example, ethanol and Cremophor EL, in the Taxol formulation. Cremophor EL has been reported as one of the factors that generate Taxol's cardiac toxicity [54]. The biodistribution results demonstrated

that drug accumulation in heart following nanocrystal administration was significantly less than that achieved with the free Taxol formulation. On the other hand, the liver appeared to tolerate high accumulation of nanocrystals, and such accumulation acted as a depot of the drug and permitted the backflow of the drug toward the plasma and consequently the tumor. The difference in the biodistribution between the two drug delivery systems suggests that, when the EPR effect offer limited benefit, a drug delivery system - as well as dosing regimen - may be better off by focusing on sparing core organs and maintaining a constant, relatively low, drug concentration in the tumor.

Second, the difference in the biodistribution between the fluorescent dye and the drug indicates that using the optical imaging for the indication of drug distribution can be limited and misleading. This is not only because of the limitation of light penetration by the IVIS system, but also due to the variation in the physicochemical properties of the two molecules such as lipophilicity, which likely lead to the differences in biodistribution and clearance, as demonstrated in our previous study in which the free dye and hybrid nanocrystals showed distinct bioimaging results [16]. As the hybrid nanocrystals started to dissolve and release the dye, the observed optical signal was a contribution of both nanocrystals and free dye molecules. The imaging probe could become more and more diverged from drug location as they further distributed.

Consequently, future development of pure and hybrid nanocrystals for cancer theranostics will focus on the control of the biodistribution in major organs. Various dosing scheme should be explored, in consulting with the absorption and clearance half-life of the drug nanocrystals, because frequent injections and/or high concentration dosing may not lead to the increase in drug concentration in the tumor but in healthy tissues and organs. Furthermore, when using hybrid nanocrystals for theranostic purposes, the biodistribution of the nanocrystals, free drug, and free probes need to be resolved and differentiated.

Acknowledgments

The project described was supported by Grant Number R25 CA153954 from the National Cancer Institute. The content is solely the responsibility of the authors and does not necessarily represent the official views of the National Cancer Institute or the National Institutes of Health.

References

1. Maeda H. Weber G. The enhanced permeability and retention (EPR) effect in tumor vasculature: The key role of tumor-selective macromolecular drug targeting. Advances in Enzyme Regulation. 2001; 41:189–207. [PubMed: 11384745]
2. Maeda H, Wu J, Sawa T, Matsumura Y, Hori K. Tumor vascular permeability and the EPR effect in macromolecular therapeutics: A review. J. Control. Release. 2000; 65:271–284. [PubMed: 10699287]
3. Jain RK. Molecular regulation of vessel maturation. Nat. Med. 2003; 9:685–693. [PubMed: 12778167]
4. Less JR, Skalak TC, Sevick EM, Jain RK. Microvascular architecture in a mammary-carcinoma - branching patterns and vessel dimensions. Cancer Res. 1991; 51:265–273. [PubMed: 1988088]
5. Bae YH, Park K. Targeted drug delivery to tumors: Myths, reality and possibility. J. Control. Release. 2011; 153:198–205. [PubMed: 21663778]
6. Daldrup H, Shames DM, Wendland M, Okuhata Y, Link TM, Rosenau W, Lu Y, Brasch RC. Correlation of dynamic contrast-enhanced MR imaging with histologic tumor grade: Comparison of macromolecular and small-molecular contrast media. Am. J. Roentgenol. 1998; 171:941–949. [PubMed: 9762973]

7. Hashizume H, Baluk P, Morikawa S, McLean JW, Thurston G, Roberge S, Jain RK, McDonald DM. Openings between defective endothelial cells explain tumor vessel leakiness. Am. J. Pathol. 2000; 156:1363–1380. [PubMed: 10751361]
8. Hobbs SK, Monsky WL, Yuan F, Roberts WG, Griffith L, Torchilin VP, Jain RK. Regulation of transport pathways in tumor vessels: Role of tumor type and microenvironment. PNAS. 1998; 95:4607–4612. [PubMed: 9539785]
9. Maeda H. Nitroglycerin enhances vascular blood flow and drug delivery in hypoxic tumor tissues: Analogy between angina pectoris and solid tumors and enhancement of the EPR effect. J. Control. Release. 2010; 142:296–298. [PubMed: 20074683]
10. Fang J, Nakamura H, Maeda H. The EPR effect: Unique features of tumor blood vessels for drug delivery, factors involved, and limitations and augmentation of the effect. Adv. Drug Deliv. Rev. 2011; 63:136–151. [PubMed: 20441782]
11. Chan HK, Kwok PCL. Production methods for nanodrug particles using the bottom-up approach. Adv. Drug Deliver. Rev. 2011; 63:406–416.
12. Müller RH, Jacobs C, Kayser O. Nanosuspensions as particulate drug formulations in therapy Rationale for development and what we can expect for the future. Adv. Drug Deliv. Rev. 2001; 47:3–19. [PubMed: 11251242]
13. Shegokar R, Müller RH. Nanocrystals: Industrially feasible multifunctional formulation technology for poorly soluble actives. Int. J. Pharm. 2010; 399:129–139. [PubMed: 20674732]
14. Liu F, Park JY, Zhang Y, Conwell C, Liu Y, Bathula SR, Huang L. Targeted cancer therapy with novel high drug-loading nanocrystals. J. Pharm. Sci. 2010; 99:3542–3551. [PubMed: 20564383]
15. Merisko-Liversidge E, Liversidge GG, Cooper ER. Nanosizing: a formulation approach for poorly-water-soluble compounds. Eur. J. Pharm. Sci. 2003; 18:113–120. [PubMed: 12594003]
16. Zhao RS, Hollis CP, Zhang H, Sun LL, Gemeinhart RA, Li TL. Hybrid nanocrystals: achieving concurrent therapeutic and bioimaging functionalities toward solid tumors. Mol. Pharm. 2011; 8:1985–1991. [PubMed: 21812439]
17. Al-Jamal WT, Kostarelos K. Liposomes: from a clinically established drug delivery system to a nanoparticle platform for theranostic nanomedicine. Acc. Chem. Res. 2011; 44:1094–1104. [PubMed: 21812415]
18. Levine DH, Ghoroghchian PP, Freudenberg J, Zhang G, Therien MJ, Greene MI, Hammer DA, Murali R. Polymersomes: A new multi-functional tool for cancer diagnosis and therapy. Methods. 2008; 46:25–32. [PubMed: 18572025]
19. Caldorera-Moore ME, Liechty WB, Peppas NA. Responsive theranostic systems: Integration of diagnostic imaging agents and responsive controlled release drug delivery carriers. Acc. Chem. Res. 2011; 44:1061–1070. [PubMed: 21932809]
20. Blanco E, Kessinger CW, Sumer BD, Gao J. Multifunctional micellar nanomedicine for cancer therapy. Exp. Biol. Med. 2009; 234:123–131.
21. Kherlopian AR, Song T, Duan Q, Neimark MA, Po MJ, Gohagan JK, Laine AF. A review of imaging techniques for systems biology. BMC Syst. Biol. 2008; 2
22. Lyons SK. Advances in imaging mouse tumour models in vivo. J. Pathol. 2005; 205:194–205. [PubMed: 15641018]
23. Montet X, Ntziachristos V, Grimm J, Weissleder R. Tomographic fluorescence mapping of tumor targets. Cancer Res. 2005; 65:6330–6336. [PubMed: 16024635]
24. Ntziachristos V, Bremer C, Weissleder R. Fluorescence imaging with near-infrared light: new technological advances that enable in vivo molecular imaging. Eur. Radiol. 2003; 13:195–208. [PubMed: 12541130]
25. Kim J-H, Kim Y-S, Park K, Lee S, Nam HY, Min KH, Jo HG, Park JH, Choi K, Jeong SY, Park R-W, Kim I-S, Kim K, Kwon IC. Antitumor efficacy of cisplatin-loaded glycol chitosan nanoparticles in tumor-bearing mice. J. Control. Release. 2008; 127:41–49. [PubMed: 18234388]
26. Koo AN, Min KH, Lee HJ, Lee S-U, Kim K, Kwon IC, Cho SH, Jeong SY, Lee SC. Tumor accumulation and antitumor efficacy of docetaxel-loaded core-shell-corona micelles with shell-specific redox-responsive cross-links. Biomaterials. 2012; 33:1489–1499. [PubMed: 22130564]
27. Lee BS, Park K, Park S, Kim GC, Kim HJ, Lee S, Kil H, Oh SJ, Chi DY, Kim K, Choi K, Kwon IC, Kim SY. Tumor targeting efficiency of bare nanoparticles does not mean the efficacy of

loaded anticancer drugs: Importance of radionuclide imaging for optimization of highly selective tumor targeting polymeric nanoparticles with or without drug. J. Control. Release. 2010; 147:253–260. [PubMed: 20624433]

28. Li C, Xia JA, Wei XB, Yan HH, Si Z, Ju SH. pH-activated near-infrared fluorescence nanoprobe imaging tumors by sensing the acidic microenvironment. Adv. Funct. Mat. 2010; 20:2222–2230.
29. Min KH, Lee HJ, Kim K, Kwon IC, Jeong SY, Lee SC. The tumor accumulation and therapeutic efficacy of doxorubicin carried in calcium phosphate-reinforced polymer nanoparticles. Biomaterials. 2012; 33:5788–5797. [PubMed: 22591612]
30. Yang Z, Leon J, Martin M, Harder JW, Zhang R, Liang D, Lu W, Tian M, Gelovani JG, Qiao A, Li C. Pharmacokinetics and biodistribution of near-infrared fluorescence polymeric nanoparticles. Nanotechnology. 2009; 20
31. Park K. Nanotechnology: What it can do for drug delivery. J. Control. Release. 2007; 120:1–3. [PubMed: 17532520]
32. Gulati M, Grover M, Singh S, Singh M. Lipophilic drug derivatives in liposomes. Int. J. Pharm. 1998; 165:129–168.
33. Mayer LD, Krishna R, Webb M, Bally M. Designing liposomal anticancer drug formulations for specific therapeutic applications. J Liposome Res. 2000; 10:99–115.
34. Barbe C, Bartlett J, Kong LG, Finnie K, Lin HQ, Larkin M, Calleja S, Bush A, Calleja G. Silica particles: A novel drug-delivery system. Adv. Mater. 2004; 16:1959–1966.
35. Moghimi SM, Hunter AC, Murray JC. Long-circulating and target-specific nanoparticles: Theory to practice. Pharmacol. Rev. 2001; 53:283–318. [PubMed: 11356986]
36. Yuan F, Dellian M, Fukumura D, Leunig M, Berk DA, Torchilin VP, Jain RK. Vascular-permeability in a human tumor xenograft - molecular-size dependence and cutoff size. Cancer Res. 1995; 55:3752–3756. [PubMed: 7641188]
37. Liu F, Park J-Y, Zhang Y, Conwell C, Liu Y, Bathula SR, Huang L. Targeted cancer therapy with novel high drug-loading nanocrystals. Journal of Pharmaceutical Sciences. 2010; 99:3542–3551. [PubMed: 20564383]
38. Eiseman JL, Eddington ND, Leslie J, Macauley C, Sentz DL, Zuhowski M, Kujawa JM, Young D, Egorin MJ. Plasma pharmacokinetics and tissue distribution of paclitaxel in CD2F1 mice. Cancer Chemother. Pharmacol. 1994; 34:465–471. [PubMed: 7923556]
39. Sparreboom A, vanTellingen O, Nooijen WJ, Beijnen JH. Tissue distribution, metabolism and excretion of paclitaxel in mice. Anticancer Drugs. 1996; 7:78–86. [PubMed: 8742102]
40. Hennenfent KL, Govindan R. Novel formulations of taxanes: a review. Old wine in a new bottle? Ann. Oncol. 2006; 17:735–749. [PubMed: 16364960]
41. Ait-Oudhia S, Straubinger RM, Mager DE. Meta-analysis of nanoparticulate paclitaxel delivery system pharmacokinetics and model prediction of associated neutropenia. Pharm. Res. 2012; 29:2833–2844. [PubMed: 22588463]
42. Rabinow B, Kipp J, Papadopoulos P, Wong J, Glosson J, Gass J, Sun CS, Wielgos T, White R, Cook C, Barker K, Wood K. Itraconazole IV nanosuspension enhances efficacy through altered pharmacokinetics in the rat. Int. J. Pharm. 2007; 339:251–260. [PubMed: 17398045]
43. Frank MM, Fries LF. The role of complement in inflammation and phagocytosis. Immunol. Today. 1991; 12:322–326. [PubMed: 1755943]
44. Owens DE, Peppas NA. Opsonization, biodistribution, and pharmacokinetics of polymeric nanoparticles. Int. J. Pharm. 2006; 307:93–102. [PubMed: 16303268]
45. Wang YL, Li XM, Wang LY, Xu YL, Cheng XD, Wei P. Formulation and pharmacokinetic evaluation of a paclitaxel nanosuspension for intravenous delivery. Int. J. Nanomed. 2011; 6:1497–1507.
46. Gao L, Zhang DR, Chen MH, Duan CX, Dai WT, Jia LJ, Zhao WF. Studies on pharmacokinetics and tissue distribution of oridonin nanosuspensions. Int. J. Pharm. 2008; 355:321–327. [PubMed: 18242896]
47. Ganta S, Paxton JW, Baguley BC, Garg S. Formulation and pharmacokinetic evaluation of an asulacrine nanocrystalline suspension for intravenous delivery. Int. J. Pharm. 2009; 367:179–186. [PubMed: 18848873]

48. Fujii T, Tachibana M, Dhar DK, Ueda S, Kinugasa S, Yoshimura H, Kohno H, Nagasue N. Combination therapy with paclitaxel and thalidomide inhibits angiogenesis and growth of human colon cancer xenograft in mice. Anticancer Res. 2003; 23:2405–2411. [PubMed: 12894521]

49. Du SZ, Zhu L, Du B, Shi XF, Zhang ZZ, Wang SY, Zhang CF. Pharmacokinetic evaluation and antitumor activity of 2-methoxyestradiol nanosuspension. Drug Dev. Ind. Pharm. 2012; 38:431–438. [PubMed: 21951208]

50. Hao LL, Wang XY, Zhang DR, Xu QY, Song SY, Wang FH, Li CY, Guo HJ, Liu Y, Zheng DD, Zhang Q. Studies on the preparation, characterization and pharmacokinetics of Amoitone B nanocrystals. Int. J. Pharm. 2012; 433:157–164. [PubMed: 22579996]

51. Liu Y, Tseng Y.-c. Huang L. Biodistribution studies of nanoparticles using fluorescence imaging: A qualitative or quantitative method? Pharm. Res. 2012; 29:3273–3277. [PubMed: 22806405]

52. Hilderbrand SA, Weissleder R. Near-infrared fluorescence: application to in vivo molecular imaging. Curr. Opin. Chem. Biol. 2010; 14:71–79. [PubMed: 19879798]

53. Pham W, Medarova Z, Moore A. Synthesis and application of a water-soluble near-infrared dye for cancer detection using optical imaging. Bioconj. Chem. 2005; 16:735–740.

54. Arbuck SG, Strauss H, Rowinsky E, Christian M, Suffness M, Adams J, Oakes M, McGuire W, Reed E, Gibbs H. A reassessment of cardiac toxicity associated with Taxol. J. Natl. Cancer Inst. Monogr. 1993; 15:117–130. [PubMed: 7912518]

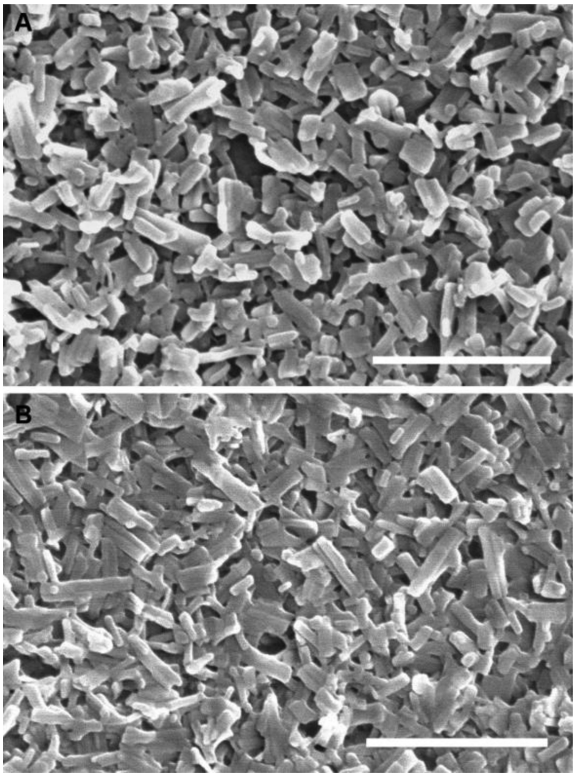

Fig. 1.
SEM images of (A) PTX pure nanocrystals for weekly intravenous injections during the survival study, (B) PTX hybrid nanocrystals without any radioactive payload. The scale bars represent 1 μm.

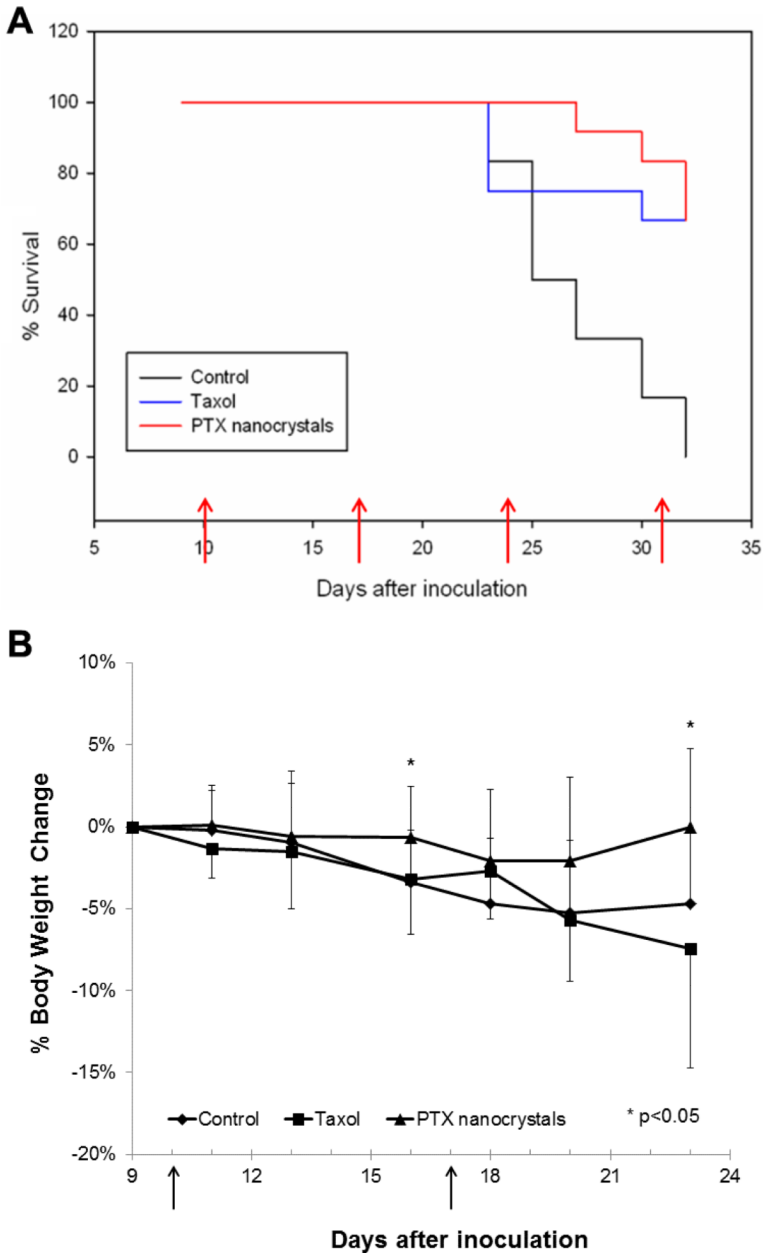

Fig. 2.

(A) The percent of animal survival versus time. Animals were administered either with saline, 20 mg/kg Taxol or PTX nanocrystals at day 10, 17, 24, and 31 after inoculation (n=12 on day 0). Tumors became palpable after nine days of inoculation (i.e. used as the plot starting points). **(B)** Percent body weight change (mean ± S.D.) of animals in three treatment groups up to day 23 after inoculation (prior to euthanization, n=12 for all the groups). The days when the injections were given are marked by arrows.

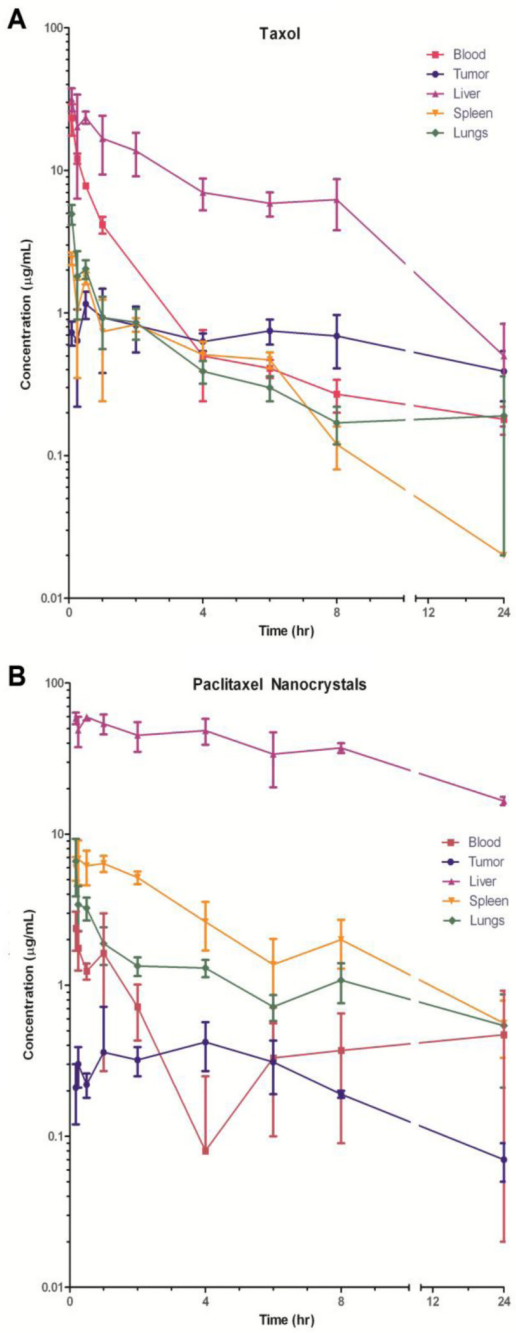

Fig. 3.

The distribution (mean ± S.D.) of ^{3}H-PTX in female nude mice after a bolus intravenous injection of (A) ^{3}H-Taxol and (B) ^{3}H-PTX/FPI-749 nanocrystals at 20 mg/kg.

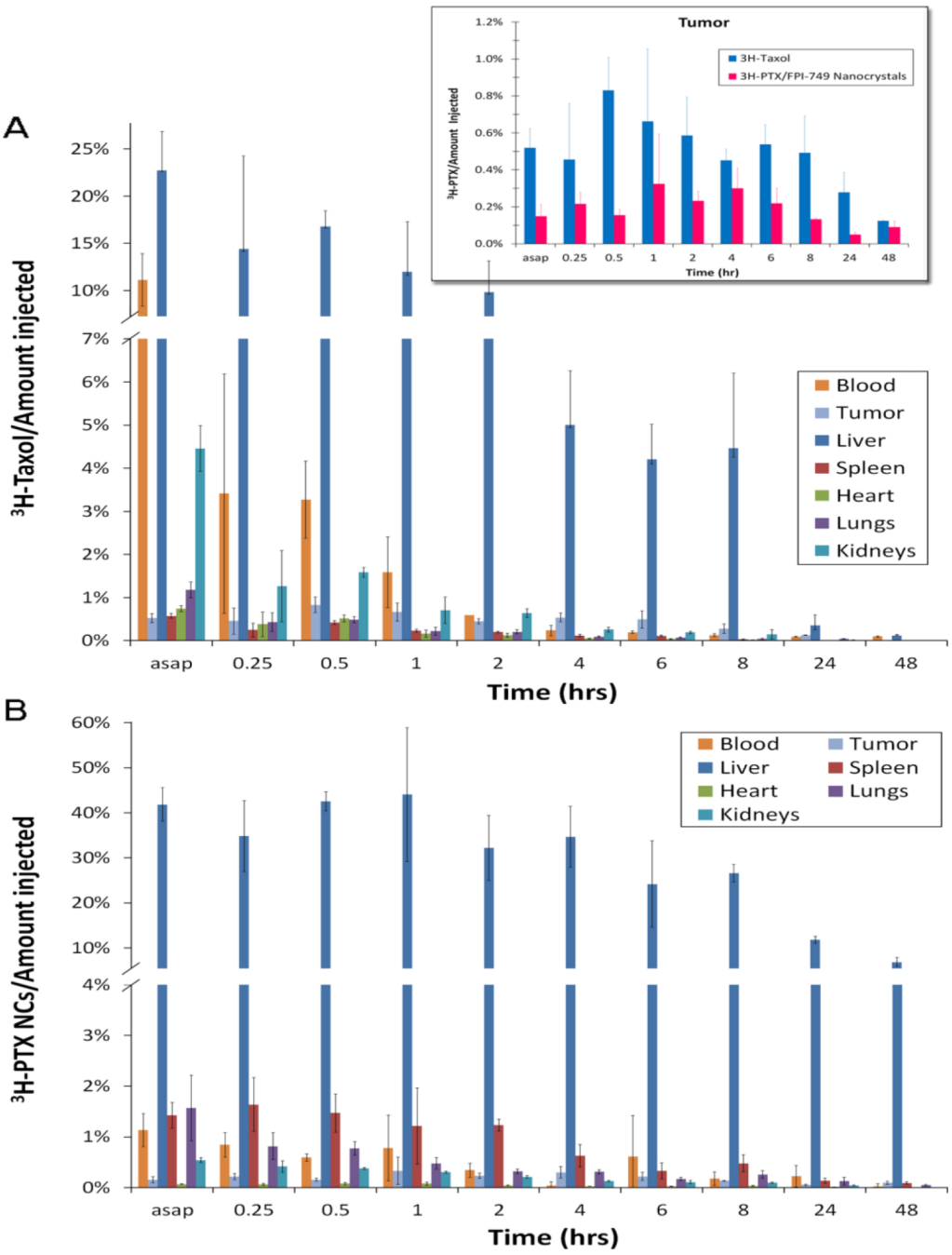

Fig. 4.

The distribution (amount in blood or tissue/amount injected; mean ± S.D.) of 20 mg/kg (A) ^{3}H-Taxol and (B) ^{3}H-PTX/FPI-749 nanocrystals. Inset: The comparison of % amount of ^{3}H-Taxol and ^{3}H-PTX/FPI-749 nanocrystals (mean ± S.D.) in tumor. In tumor, ^{3}H-Taxol was significantly higher than that of ^{3}H-PTX nanocrystals regardless the time point ($p < 0.0001$). The term “asap” refers to 5 and 11 minutes post-injection time of ^{3}H-Taxol and ^{3}H-PTX/FPI-749 nanocrystals, respectively.

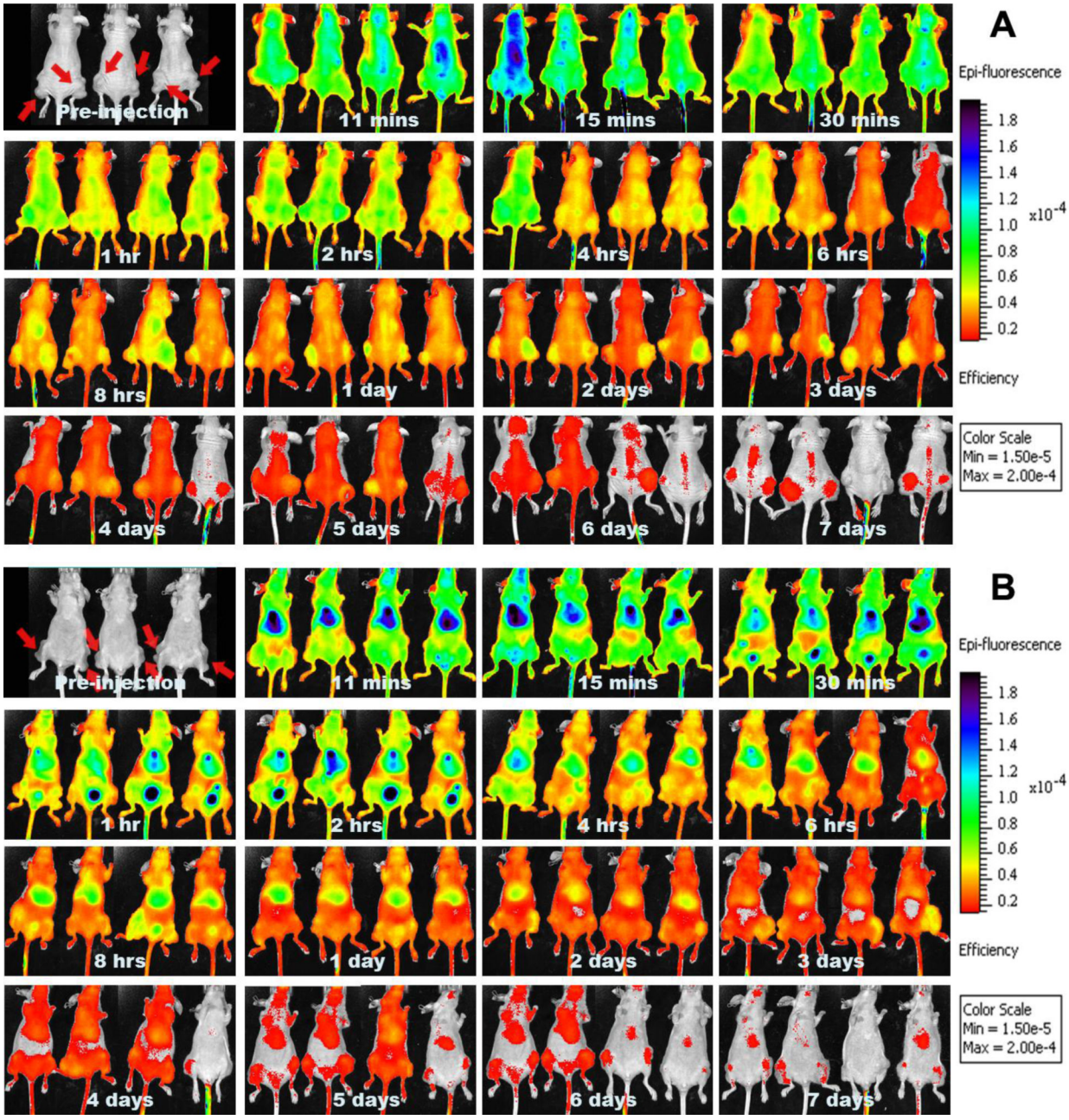

Fig. 5.

IVIS® images of athymic mice injected with ^{3}H-PTX/FPI-749 nanocrystals from (A) dorsal and (B) ventral views. Tumors are marked in the images of pre-injection.

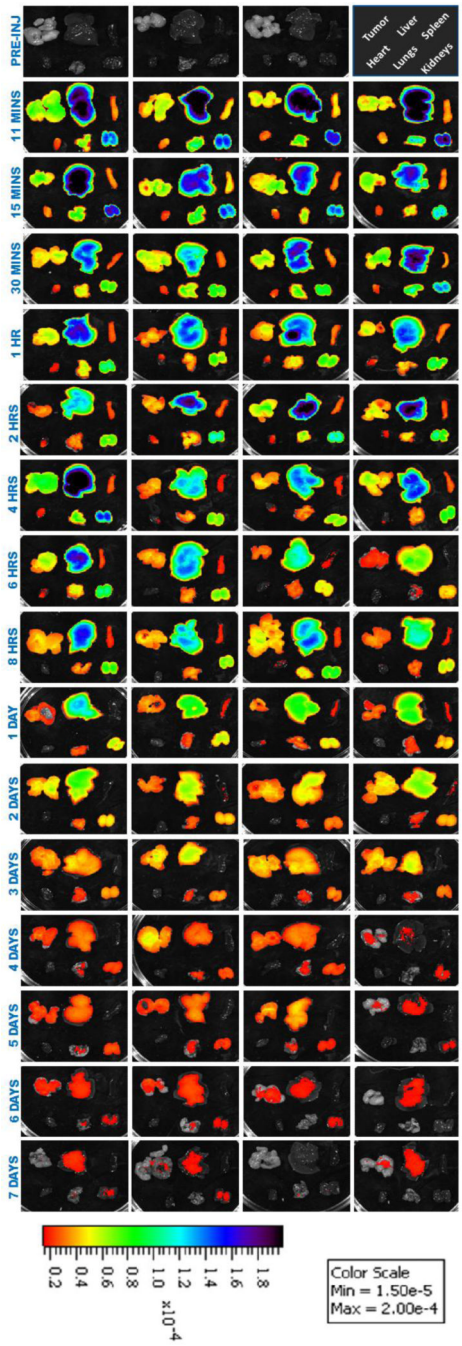

Fig. 6.

IVIS® images of ex-vivo tissues of animals administered with ^{3}H-PTX/FPI-749 nanocrystals.

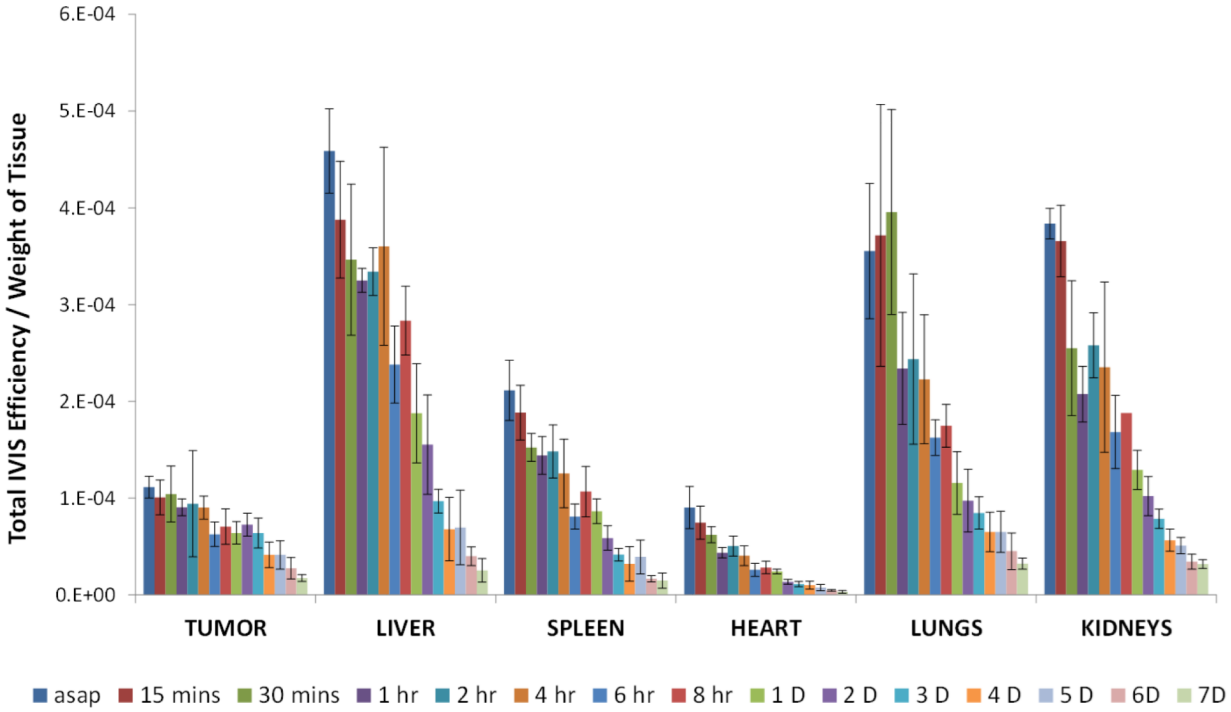

Fig. 7.

The fluorescence distribution (total efficiency (cm^2)/gram of blood or tissue, mean ± S.D.) of 20 mg/kg ^{3}H-PTX/FPI-749 nanocrystals. The term "asap" refers to 11 minutes post-injection time.

Table 1

The physical characterizations (mean ± S.D.) of PTX nanocrystals used during the survival study.

Properties	Paclitaxel nanocrystals			
	Injection 1	Injection 2	Injection 3	Injection 4
Particle size (SigmaScan) (nm)	149 ± 44	198 ± 63	193 ± 63	195 ± 62
Hydrodynamic diameter (DLS) (nm)	179 ± 1	200 ± 4	197 ± 3	198 ± 2
Polydispersity Index	0.25 ± 0.01	0.16 ± 0.02	0.15 ± 0.04	0.17 ± 0.04